Bond-breakage-dependent dissociative ionization of an asymmetric molecule in an intense femtosecond laser field

Pan Ma,[1,2] Chuncheng Wang,[1,2,*] Sizuo Luo,[1,2] Xiaokai Li,[1,2] Wenhui Hu,[1,2] Jiaqi Yu,[1,2] Xitao Yu,[1,2] Xu Tian,[1,2] Zexing Qu,[3,*] and Dajun Ding[1,2,*]

[1]*Institute of Atomic and Molecular Physics, Jilin University, Changchun 130012, People's Republic of China*

[2]*Jilin Provincial Key Laboratory of Applied Atomic and Molecular Spectroscopy, Jilin University, Changchun 130012, People's Republic of China*

[3]*Theoretical Chemistry Institute, Jilin University, Changchun 130012, People's Republic of China*

(Received 17 October 2018; published 19 February 2019)

A coincidence momentum imaging method is used to investigate the dissociative ionization of carbonyl sulfide (OCS) irradiated by linearly polarized 800 nm femtosecond laser pulses. As a typical asymmetric molecule, kinetic-energy release (KER) distributions of two-body Coulomb explosion (CE) along C-S or C-O bond breakage from OCS^{q+} ($q = 2, 3, 4$) exhibit a different behavior when the parent charge state increases. Two processes, i.e., concerted enhanced multiple ionization and ladder-climbing-type sequential ionization, are proposed for the C-S and C-O bond breakage, respectively. With the help of the potential-energy curves (PEC) obtained from the multistate density-functional-theory method, the KER values are calculated for these CE channels of OCS^{q+}. The overall good quantitative agreement between the experiment and calculation confirms the validity of the ionization mechanism assumed. In our approach, the global minimum of cationic PEC for the OCS can be treated as R_c for enhanced ionization. Furthermore, a bimodal KER distribution was observed for the channel of $OCS^{2+} \rightarrow O^+ + CS^+$, and with the help of PEC, we believe that both of the ionization processes are involved in the dynamics of its formation.

DOI: 10.1103/PhysRevA.99.023423

I. INTRODUCTION

Strong-field-induced multiple ionization of molecules has been intensively investigated, particularly because it triggers complex ultrafast electron-nuclei motion [1–3]. Removal of one or more electrons from a molecule may alter the potential-energy surface (PES) on which the nuclei moves, resulting in bond breakage or bond formation. Meanwhile, the nuclear motion reconstructs the distribution of the remaining electrons, which dramatically influences further multiple-ionization dynamics in a strong laser field. It is therefore critical to understand the mechanism of dissociative multiple ionization [4–6] along different bond stretches, especially for asymmetric molecules.

The essential role of coupling between nuclei movement and electron ionization has been confirmed by the studies of diatomic molecules, whose double-ionization rate exhibit a dramatic enhancement at a certain internuclear distance when the molecular axis is parallel to the field vector [7–10]. The electron at this critical distance R_c can tunnel into the continuum through the field-suppressed intramolecular potential barrier when the electronic density is localized on the upper potential well, which is the so-called enhanced ionization (EI). EI has been widely used in explaining numerous experimental works for triatomic molecules, hydrocarbon molecules, and even clusters [11–14], and it can qualitatively well explain most observations; however, R_c can only be extracted from measured kinetic-energy release (KER) by assuming pure Coulomb potential, which is a rough approximation for polyatomic molecules. Moreover, the strong-field-induced dissociative ionization of asymmetric molecules has not yet been thoroughly studied, especially for the multiple-ionization processes. Dehghanian *et al.* [15] studied the enhanced ionization and excitation of the nonsymmetric HeH^+ molecule driven by an intense laser pulse by solving the three-dimensional time-dependent Schrödinger equation. They determined that EI is suppressed when the permanent dipole moment of the molecule is parallel to the electric field of the laser pulse. This is because the electron must tunnel a much wider lifted potential barrier to reach the continuum or the absence of the coupling of the ground state and excited states in this situation [7,8].

Furthermore, Kawata *et al.* [16] predicted that the response of H_3^+ to a laser field can be classified into two regimes. In the adiabatic regime ($R < R_c$), the electron transfers from one end of the molecule to the other end every half optical cycle. In the diabatic regime ($R > R_c$), internuclear electron transfer is suppressed on account of electron repulsion and laser-induced electron localization. The ionization dynamics of this molecule depend heavily on both the electron distribution along the molecule and the nonadiabatic transitions between the lowest three electronic states. OCS is a typical asymmetric molecule. Accordingly, its ionization and dissociation have been researched with synchrotron radiation, particle collision, and the intense laser pulse [17–22]. Bryan *et al.* [23] investigated three-body Coulomb explosion (CE) of highly charged carbonyl sulfide (OCS) by the covariance

*ccwang@jlu.edu.cn; zxqu@jlu.edu.cn; dajund@jlu.edu.cn

mapping technique. They identified the existence of two sets of ionization pathways. Only one of them can be modeled using the EI model. It was noted that molecular excitation and multielectronic processes must be considered; nevertheless, a quantitative explanation was lacking. Recently, Sakemi *et al.* [24] measured molecular-frame photoelectron angular distributions of different channels for laser-induced dissociative ionization. They verified that the OCS molecules are more likely to be ionized when the electric field points toward the O atom for the production of O^+. The above theoretical and experimental studies involved the proposal of uniquely interesting ionization and dissociation features of asymmetric molecules. In particular, the multiple dissociative ionization mechanism along the C-S or C-O bond breakage for OCS is expected to be different; however, direct experimental research is still needed.

In this paper, we present an experimental study of dissociative ionization (DI) of the OCS molecule and the verification of all two-body CE channels from the parent ion OCS^{q+} ($q = 2, 3, 4$). The enhanced ionization model can explain the CE along the C-S stretch. In addition, a ladder-climbing-type sequential multiple-ionization process is proposed for the CE along the C-O stretch. The potential-energy curves (PEC) for those CE channels are calculated with the multistate density-functional-theory (MSDFT) method to calculate the theoretical KER. The overall good quantitative agreement between the experimental and theoretical results confirms the validity of the proposed mechanism and reveals possible nuclei dynamics during the DI. R_c for EI is obtained from the global minimum of PEC for the cation state. Moreover, the bimodal KER distribution of the ($O^+ - CS^+$) channel can be interpreted as the coexistence of sequential and enhanced ionization processes since there are two minima in PES along the C-O stretch of OCS^+.

II. EXPERIMENTAL AND THEORETICAL METHODS

Laser pulses of 800 nm with a pulse duration of 50 fs and repetition rate of 1 kHz produced from a Ti:sapphire laser system were used to irradiate the targets [25,26]. The linearly polarized laser beam was focused by a concave mirror ($f = 7.5$ cm) onto a supersonic OCS gas jet (seeded by helium) inside the vacuum chamber (base pressure, 1.8×10^{-10} mbar). Cold-target recoil-ion momentum spectroscopy (COLTRIMS) [27] was used to confirm the two-body CE channels. Further details are presented in our previous publications [2,28]. Briefly, the intense laser pulses interacted with targets and produced ion fragments, which were accelerated to the DLD80 detector by a uniform electric field (38.6 V/cm). Three-dimensional momenta of fragment ions could be retrieved from the measured position and time of flight. The ion count rate in all experiments was controlled below 0.4 per pulse to keep the false-coincidence rate low. Additionally, the strict momentum-conservation rule was consistently used to exclude the false-coincidence events. The laser intensity was calibrated by the ratio of Xe^{2+}/Xe^+ and compared with the previous measurement results [29].

A hybrid of the wave function and density functional theory, denoted as the MSDFT method, was used to calculate the potential-energy curves of OCS^{q+} [30,31]. In this approach, the diabatic states are defined by block-localized Kohn-Sham (BLKS) orbitals according to the bond-breakage products. BLKS orbitals constrain the electron density for each diabatic state in the orbital space. Specifically, for C-S bond breaking, the atomic basis functions are conveniently divided into two blocks: one block on CO and one block on S. The charge (or elections) can be localized on two blocks to represent different diabatic states. The adiabatic ground and excited states are yielded through the diagonalization of the configuration-interaction (CI) Hamiltonian. All the theoretical calculations were computed using the Perdew-Burke-Ernzerhof (PBE0) functional at the aug-cc-pVTZ level and implemented in our local modified general atomic and molecular electronic structure system (GAMESS) package.

III. RESULTS AND DISCUSSION

The multiple-charged OCS can dissociate through two-body CE along the C-S bond or C-O bond. We employed the ion-ion coincidence method to extract all two-body CE channels, as shown in Fig. 1. Each narrow parabolic line in the figure represents a CE channel, which is unambiguously identified by applying the momentum-conservation conditions. The color scale represents the relative yields of each channel. These channels are classified into two groups according to their bond breakage, $CO^{m+} + S^{n+}$ or $O^{r+} + CS^{s+}$ group (m, n, r, and s represent the charge of the fragment ions), as shown in (1) to (8).

The C-S bond-breakage group is

$$OCS^{2+} \rightarrow CO^+ + S^+, \quad (1)$$

$$OCS^{3+} \rightarrow CO^+ + S^{2+}, \quad (2)$$

$$OCS^{3+} \rightarrow CO^{2+} + S^+, \quad (3)$$

$$OCS^{4+} \rightarrow CO^+ + S^{3+}. \quad (4)$$

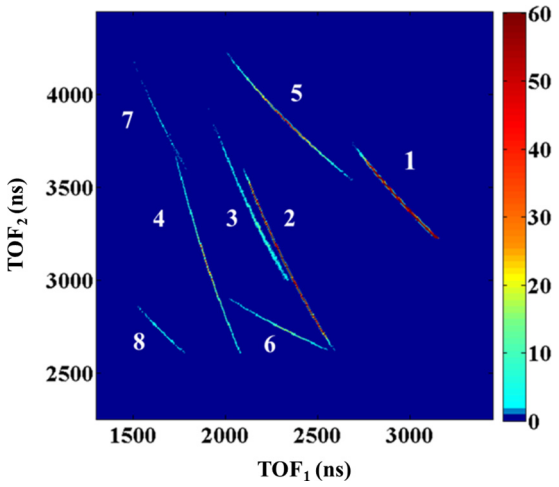

FIG. 1. Photo-ion and photo-ion coincidence (PIPICO) spectrum obtained from the interaction of linearly intense femtosecond laser pulses (1.2 PW/cm^2). Eight two-body CE channels are shown. Labeled numbers represent the channels as follows: 1: $CO^+ + S^+$; 2: $CO^+ + S^{2+}$; 3: $CO^{2+} + S^+$; 4: $CO^+ + S^{3+}$; 5: $O^+ + CS^+$; 6: $O^+ + CS^{2+}$; 7: $O^{2+} + CS^+$; and 8: $O^{2+} + CS^{2+}$. The color map indicates the ion yield for each channel.

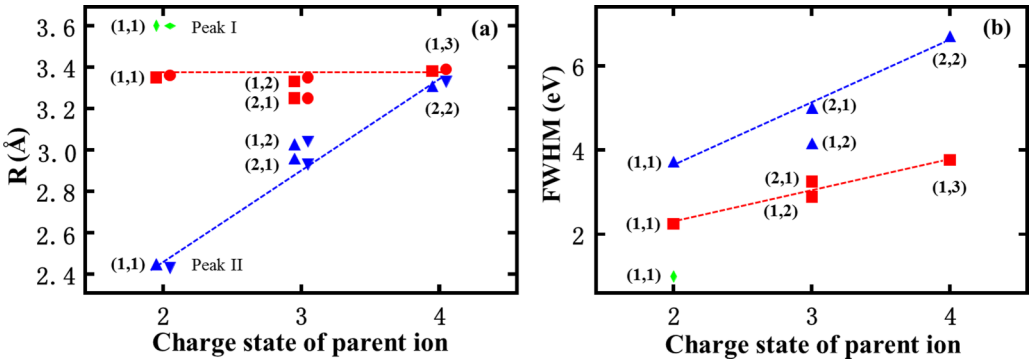

FIG. 2. Experimentally deduced distance (R) of two fragments before CE is shown as the increase of the charge state of the parent ions. (a) Red squares and circles denote $CO^{m+} + S^{n+}$ channels; blue straight and inverted triangles represent $O^{r+} + CS^{s+}$ channels with the intensity of 0.5 and 1.2 PW/cm^2, respectively. The nuclear distance R calculated from the lower (peak I) and larger (peak II) energy components of channel (5) are also shown as a green diamonds and blue triangles, respectively. The marks (m, n) and (r, s) denote the charge distribution of each channel. (b) The corresponding FWHM of KERs for each channel in (a) with the intensity of 0.5 PW/cm^2.

The C-O bond-breakage group is

$$OCS^{2+} \rightarrow O^{+} + CS^{+}, \tag{5}$$

$$OCS^{3+} \rightarrow O^{+} + CS^{2+}, \tag{6}$$

$$OCS^{3+} \rightarrow O^{2+} + CS^{+}, \tag{7}$$

$$OCS^{4+} \rightarrow O^{2+} + CS^{2+}. \tag{8}$$

The overall ion-pair yields for channels (5)–(8) were much lower than those for channels (1)–(4). We obtained the KERs and momentum distributions for all the CE channels, and then further extracted the distance R between the mass centers of two fragments just before the CE according to the simple CE model [Fig. 2(a)]. From the measured KER distributions, we deduced their full width at half maximum (FWHM) for all the channels as the charge state increased from 2 to 4, as shown in Fig. 2(b). The values of R for all the channels are plotted in Fig. 2(a) for the increasing parent-ion charge state from two to four. It is clear that the changes of R values with the increasing charge state are very different for the respective C-S and C-O bond breakages. That is, the value of R scarcely changes (approximately 3.3 Å) for the C-S bond breaking, whereas it increases for the C-O bond breakage from 2.3 to 3.2 Å as the parent charge state increases from 2 to 4. In the classical enhanced ionization model [7,10], the constant R for C-S bond breakage can be treated as the critical distance R_c. After removing one electron from neutral OCS, the C-S bond of the cations begins to extend from the equilibrium distance R_e to R_c and leads to electron localization. Then, one or few electrons can be immediately removed through laser-field-induced tunneling ionization in a concerted manner. However, for C-O bond breakage, the R value is almost linearly extended as the charge states increase from 2 to 4, which cannot be explained by EI.

At the same time, the asymmetric nature of OCS may lead to a high charge-asymmetric distribution for CE channels, which also relies on the bond breakage. From the same parent-ion state OCS^{4+}, the high charge-asymmetric channel (1, 3) is dominant for C-S bond breakage, and only the charge-symmetric channel (2, 2) for C-O bond breakage is observed. In contrast, both (1, 3) and (2, 2) channels were observed for C-S bond breakage by Bommer *et al.* using a synchrotron radiation source [32]. We thus infer that the strong-field-induced electron localization effect may influence these bond-breakage-dependent charge-asymmetric distributions of the CE channel. Within the enhanced ionization model, multiple ionization may occur in a concerted way at a larger critical distance R_c with electron localization, and then the electron is easily ionized from the S site [33]. Thus, the electron transfer along the molecular bond may be strongly prohibited and the charge-symmetric channel suppressed, as suggested by Kawata *et al.* based on the calculation of H_3^+ [16]. However, the DI along the C-O bond may proceed through a sequential process, and the C-O bond extension is not large enough for electron localization; thus, electron transfer along the molecular bond may still play an essential role, which enhances the yield of the charge-symmetric channel (2, 2). These observations scarcely rely on the laser intensities. In the case of N_2, the charge-asymmetric channel (3,1) is strongly suppressed at critical distance R_c [34] because N^+ is much more easily ionized than N^{2+} after electron localization, and the author claimed that this was direct evidence for the electron localization in EI of the symmetry molecule. This issue is consistent with our observations for asymmetric molecule OCS; electron localization along the C-S stretch enhanced the ionization from S^{2+} to S^{3+} because of its relatively lower ionization potential compared to CO^+. This effect was absent for sequential ionization along the process of the C-O stretch.

The DI of the molecules has been extensively studied; however, most results only provide a qualitative analysis by assuming the pure Coulomb potential for the CE model. This is because the accurate calculation of PEC is very expensive or even impossible. Here, we intend to provide a quantitative explanation for our measured KER distribution by calculating the PEC for the CE channels up to OCS^{4+}. The density functional theory is a less expensive electronic structure method with high accuracy. However, it fails for the bond-breaking process owing to the well-known problem of the fractional spin error [35]. We recently developed the MSDFT

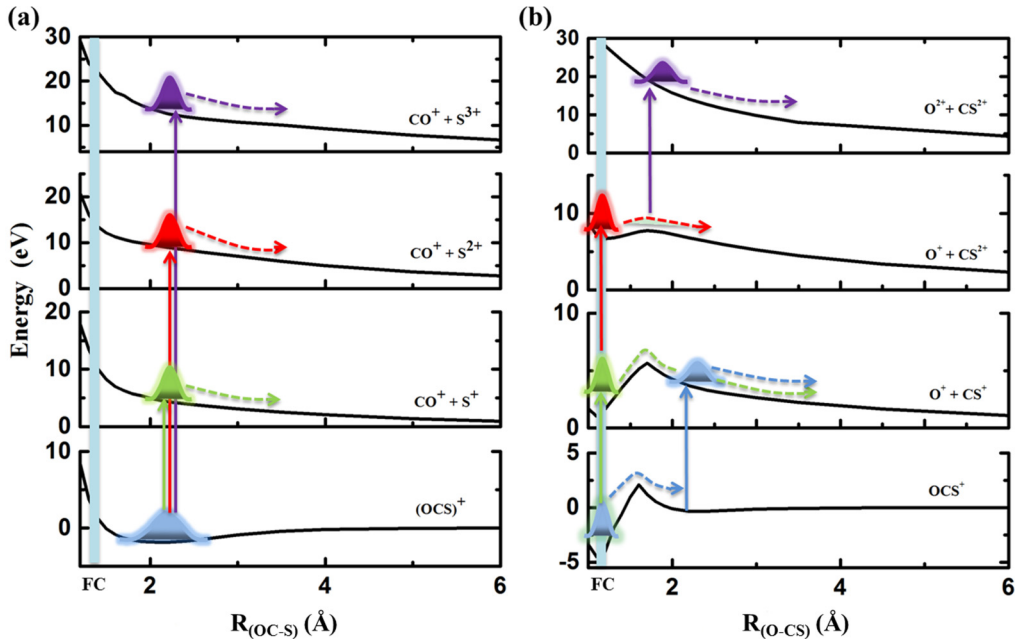

FIG. 3. Potential-energy curves of dissociative channels of OCS^{q+} ($q = 1-4$) along the (a) C-S stretch and (b) C-O stretch. Solid arrows refer to the scheme of (a) the concerted enhanced ionization mechanism starting from the minima of PEC of the cation state along the C-S stretch and (b) the sequential vertical multiple-ionization process originating from the minima of each charge state (1–3) along the C-O stretch. The dashed arrows denote the possible movement of nuclei wave packets.

and diabatic-at-construction (DAC) strategy to overcome this problem and compute the diabatic and adiabatic states at the same root [30,31]. The calculated PECs using this method for the main CE channels from OCS^{q+} ($q = 1-4$) along the C-S and C-O stretches are shown in Fig. 3. The PECs along the C-S stretch are nearly Coulombic for OCS^{q+} ($q = 2-4$), while deep potential wells exist around 1.0–1.3 Å for OCS^{q+} ($q = 1-3$) along the C-O stretch. For the cation state, the minimum of the PEC along the C-S stretch is located at ∼2.2 Å, which is larger than the equilibrium C-S bond distance (1.56 Å). Thus, the nuclei wave packet may intend to evolve toward this minimum from the Frank-Condon region, and the so-called R_c can be possibly reached along the C-S bond through the bond extension for this cation state. At this position, the enhanced ionization may proceed through field ionization to the higher charge state. The PECs of dication, trication, and tetravalent cation are all Coulombic and the molecular ions may immediately dissociate along those curves. Then, the CE occurs nearly at the same position of R_c, which is consistent with our observation in Fig. 2(a).

Along the C-O stretch in Fig. 3(b), the minimum of the cation PEC is located at ∼1.1 Å, which is almost the same as its equilibrium bond distance (1.15 Å). This well may inhibit the significant bond extension, which leads to the suppression of enhanced ionization along this C-O stretch. Thus, further ionization to the dication state mainly occurs through vertical ionization around the Frank-Condon region. The CE from the dication state along the C-O bond breakage must overcome a potential barrier. Accordingly, more photons may need to be absorbed for the excitation of vibrational wave packets, and the molecule may finally cross the barrier where the CE occurs. We name this DI process as ladder-climbing-type sequential ionization. The CE from the trication state may also follow this ladder-climbing-type dissociative ionization mechanism along the C-O stretch. Therefore, our calculations confirm that the pure Coulombic or non-Coulombic PEC of OCS^{q+} along the C-S or C-O stretch lead to the concerted EI or ladder-climbing-type multiple DI processes. Moreover, we observe an overall broader FWHM of the $(O^{r+} + CS^{s+})$ group than the $(CO^{m+} + S^{n+})$ group, as shown in Fig. 2(b). The FWHM of the KER distribution is affected by the shape of the potential-energy curves. The deeper potential well may contain more vibrational states, which leads to a broader FWHM [36]. The calculated overall deeper potential well for each stage by photon absorption for the $(O^{r+} + CS^{s+})$ group than the $(CO^{m+} + S^{n+})$ group can effectively elucidate our observation.

Furthermore, we can deduce the kinetic-energy release from the PEC of each CE channel according to the proposed mechanism and quantitatively compare them with the measurement. As shown in Fig. 3(a), the position of the minimum of the cation PEC can be assumed as R_c. In addition, the calculated peak values of KER for $(CO^{m+} + S^{n+})$ are the difference between the potential energy at R_c and the dissociation limit for each charge state. For the $(O^{r+} + CS^{s+})$ group, the KER value can be calculated from the potential-energy difference between the barrier position and dissociation limit. The calculated and measured KER values are compared in Table I. The deviations between them for the $(CO^{m+} + S^{n+})$ group are less than 5%, which shows quite a good quantitative agreement. This excellent consistency strongly supports our proposed concerted EI mechanism for the $(CO^{m+} + S^{n+})$ group. More importantly, based on our calculation, R_c can be treated as the global minimum position of PEC along the C-S stretch for the cation state, which provides an intuitive interpretation for this critical distance for EI of the polyatomic molecule. For

TABLE I. Direct comparison of experimental and theoretical deduced KERs according to our proposed DI mechanism along the C-S and C-O stretches.

Channel	Experimental Results 0.5 PW/cm^2	Experimental Results 1.2 PW/cm^2	Theoretical Calculation
	C-S bond breakage		
1. $CO^+ + S^+$	4.3	4.3	4.5
2. $CO^+ + S^{2+}$	8.7	8.6	9.2
4. $CO^+ + S^{3+}$	12.8	12.6	13.0
	C-O bond breakage		
5. $O^+ + CS^+$	4.0(I)/5.9(II)	4.0(I)/5.9(II)	3.5(I)/5.7(II)
6. $O^+ + CS^{2+}$	9.5	9.5	7.7 (10.1)[a]
8. $O^{2+} + CS^{2+}$	17.4	17.2	19.1

[a]Deduced KER from diabatic PEC.

the $(O^{r+} + CS^{s+})$ group, a reasonable agreement for channels (5) and (8) is still achieved, although not as well as for the $(CO^{m+} + S^{n+})$ group. The calculated KER is lower than the experimental one for channel (6). The agreement can be improved by considering the diabatic PEC, which is not shown in Fig. 3. The calculated PECs we used here did not simultaneously consider the elongation of both C-S and C-O bonds, which may occur during the C-O bond breakage and lead to the KER deviation from experiment.

We are unable to deduce the KER from the PEC for channels (3) and (7), which also have a rather low yield in the measurement. This may be because the calculated PEC do not include all the contributions of excited states that may have a strong influence on those weak channels. This can also have a contribution to the relatively larger deviations for the $(O^{r+} + CS^{s+})$ group. For channel (8), vertical ionization from OCS^{3+} to OCS^{4+} at the Frank-Condon (FC) region becomes difficult since the ionization potential is quite high. The ionization may occur during the C-O bond extension along the PEC of OCS^{3+} before CE. Thus, we approximately deduce the minimum KER value from the potential-energy difference between the barrier position where the CE occurs for OCS^{3+} and the dissociation limit of OCS^{4+} [purple arrow in Fig. 3(b)], and the deduced KER value reasonably agreed with the measurement.

Furthermore, as shown in Fig. 4, channel (5) ($OCS^{2+} \rightarrow O^+ + CS^+$) has a bimodal KER distribution (black circles). The two components can be obtained through a two-peak fitting procedure. They are respectively labeled as peak I and peak II. The KER distribution of channel (1) ($OCS^{2+} \rightarrow CO^+ + S^+$) (red squares) is also inserted for comparison. Peak I of channel (5) is around 4.0 eV and peak II is around 5.9 eV. Their corresponding R values are respectively shown in Fig. 2(a), where the low-energy component corresponds to an even larger value of R (green diamond) than in channel (1). At the same time, the FWHM of the low-energy component is also much smaller than its high-energy component, as shown in Fig. 2(b). This indicates that the dramatic C-O bond extension before double ionization may also play a role for this particular channel.

Induced by electron collision at energy of 500 eV, Shen *et al.* [18] also observed this type of bimodal peak for channel (5) with kinetic energy of 4.3 and 7 eV and they roughly ascribed them to the contribution of the $3\,^3\Sigma^-$ state of the $2\pi^{-1}\,3\pi^{-2}\,4\pi^1$ configuration and the $1\,^5\Pi$ state of the $9\sigma^{-1}\,3\pi^{-2}\,4\pi^1$ configuration, respectively. Ramadhan *et al.* [17] found the bimodal peak locating at 5 and 10 eV for channel (5) with synchrotron radiation, and they attributed them to the contributions of several different electronic states. Here, this bimodal KER distribution for channel (5) is observed in strong-field-induced CE, and the interpretation based on the multiple excited states' contribution cannot give reasonable quantitative agreement between experiment and calculation without the exact PEC. Here we propose that peaks I and II may have a different underlying mechanism. The PEC along the C-O stretch of the OCS cation in Fig. 3(b) exhibits not only a deep potential well at the FC region, but also a second shallow potential well around 2.1 Å. The C-O bond extension may reach the second shallow potential well through vibration excitation or the coupling of excited states. Then, further ionization may occur at this distance through the enhanced

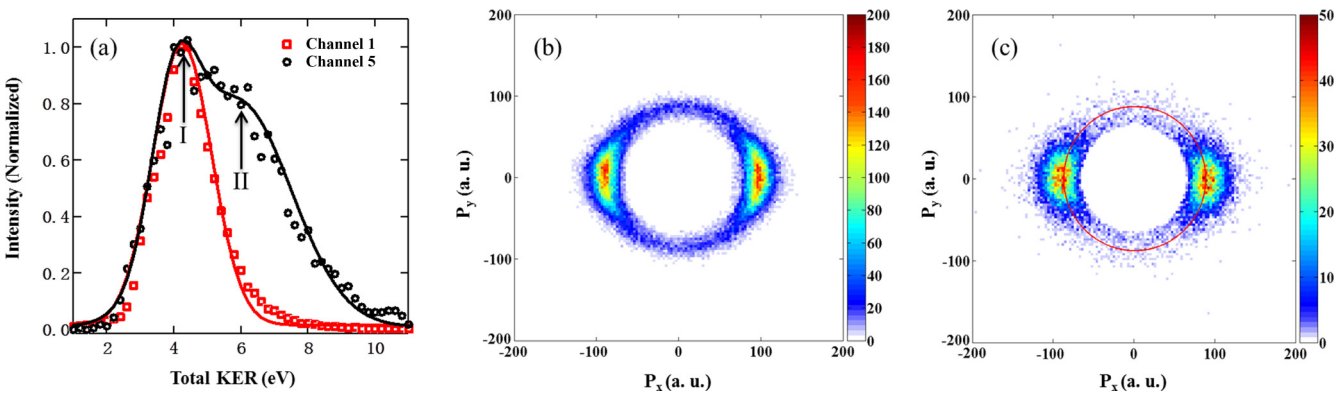

FIG. 4. (a). Bimodal KER distributions of channel (5) $O^+ + CS^+$ at the intensity of 0.5 PW/cm^2 are shown as black circles. The KER distribution of channel (1) $CO^+ + S^+$ is inserted (red squares) for comparison. The red and black solid lines represent the Gaussian fitting results. The two-peak fitting curves for channel (5) and its lower-energy component are similar to the value of channel (1). (b), (c) The momentum angular distributions for channel (1) and channel (5), respectively. P_x stands for the momentum of the fragment along the laser polarization direction. The red solid ring in (c) represents the momentum corresponding to peak I in (a).

ionization mechanism, as indicated in Fig. 3(b) (dashed line). From this position, we can deduce the KER from the PEC of OCS dication. The calculated values have a good quantitative agreement with the measurement (shown in Table I), indicating the validity of our interpretation. Interestingly, peak I has a very similar KER distribution and FWHM value as channel (1). We believe that the same enhanced ionization mechanism and similar critical distance (2.1 and 2.2 Å, respectively) lead to nearly identical KER distributions along the different bond breakages. As discussed in the previous paragraph, peak II mainly come from the ladder-climbing-type sequential double-ionization process. The fragment's momentum angular distributions of channel (1) and channel (5) have been shown in Figs. 4(b) and 4(c). The fragments of channel (1) mainly ejected along the laser polarization direction, which gives typical anisotropic distributions for two-body CE through enhanced ionization. This angular distribution can be correlated with the molecular alignment, multiple orbital ionization, and different ionization mechanisms, which have been widely discussed before [5,37,38]. Channel (5) shows overall stronger anisotropic distribution since the ladder-climbing-type sequential ionization has much higher threshold intensities. Looking into the details of Fig. 4(c), the angular distribution for higher-energy fragments is slightly more anisotropic than low-energy fragments (divided by the red solid circle, which corresponds to peak I). The lower-energy region has a similar pattern of angular distribution as channel (1), which may support that peak I come from the same enhanced ionization mechanism.

IV. CONCLUSION

In summary, we studied the DI of asymmetric molecules OCS by measuring the evolution of KER distributions with the increasing charge state using the CE imaging method. We observed that the DI dynamics strongly relies on the C-S or C-O bond breakage. By combining the PEC and the proposed mechanism for different bond breakage, the calculated KERs showed overall good quantitative agreement with the measurement. This finding supports our conclusion that the concerted enhanced ionization and the ladder-climbing-type sequential ionization dominate the DI for C-S bond breakage and C-O bond breakage, respectively. Moreover, EI can also contribute to the ($OCS^{2+} \rightarrow O^{+} + CS^{+}$) channel because of the existence of local minima of the cation PEC along the C-O stretch, and this issue was confirmed by the good agreement of the KER between the calculation and measurement. Our results thus interpret the bond-breakage-dependent dissociative dynamics of the asymmetric molecule OCS in a quantitative manner and offer a way to understand strong-field-induced polyatomic molecular DI.

ACKNOWLEDGMENTS

This work was supported by the National Basic Research Program of China (973 Program) Grant No. 2013CB922200, the National Natural Science Foundation of China (Grants No. 11534004, No. 11774130, No. 11627807, No. 11304117, No. 11374122) and by the China Postdoctoral Science Foundation under Grants No. 2013M530137 and No. 2015T80293.

[1] M. Meckel, D. Comtois, D. Zeidler, A. Staudte, D. Pavičić, H. C. Bandulet, H. Pépin, J. C. Kieffer, R. Dörner, D. M. Villeneuve, and P. B. Corkum, Science **320**, 1478 (2008).
[2] P. Ma, C. Wang, X. Li, X. Yu, X. Tian, W. Hu, J. Yu, S. Luo, and D. Ding, J. Chem. Phys. **146**, 244305 (2017).
[3] M.-Z. Li, G.-R. Jia, and X.-B. Bian, J. Chem. Phys. **146**, 084305 (2017).
[4] P. Ma, C. Wang, S. Luo, X. Yu, X. Li, Z. Wang, W. Hu, J. Yu, Y. Yang, X. Tian, Z. Cui, and D. Ding, J. Phys. B **51**, 094002 (2018).
[5] C. Wang, B. Wang, M. Okunishi, W. G. Roeterdink, D. Ding, R. Zhu, G. Prümper, K. Shimada, and K. Ueda, Chem. Phys. **430**, 40 (2014).
[6] C. Wang, D. Ding, M. Okunishi, Z.-G. Wang, X.-J. Liu, G. Prümper, and K. Ueda, Chem. Phys. Lett. **496**, 32 (2010).
[7] G. L. Kamta and A. D. Bandrauk, Phys. Rev. Lett. **94**, 203003 (2005).
[8] G. L. Kamta and A. D. Bandrauk, Phys. Rev. A **76**, 053409 (2007).
[9] X.-B. Bian, L.-Y. Peng, and T.-Y. Shi, Phys. Rev. A **77**, 063415 (2008).
[10] S. Chelkowski, T. Zuo, O. Atabek, and A. D. Bandrauk, Phys. Rev. A **52**, 2977 (1995).
[11] H. Chen, V. Tagliamonti, and G. N. Gibson, Phys. Rev. A **86**, 051403(R) (2012).
[12] I. Bocharova, R. Karimi, E. F. Penka, J.-P. Brichta, P. Lassonde, X. Fu, J.-C. Kieffer, A. D. Bandrauk, I. Litvinyuk, J. Sanderson, and F. Légaré, Phys. Rev. Lett. **107**, 063201 (2011).
[13] E. Lötstedt, T. Kato, and K. Yamanouchi, Phys. Rev. A **85**, 041402 (2012).
[14] C. Siedschlag and J. M. Rost, Phys. Rev. A **67**, 013404 (2003).
[15] E. Dehghanian, A. D. Bandrauk, and G. L. Kamta, J. Chem. Phys. **139**, 084315 (2013).
[16] I. Kawata, H. Kono, and A. D. Bandrauk, Phys. Rev. A **64**, 043411 (2001).
[17] A. Ramadhan, B. Wales, R. Karimi, I. Gauthier, M. MacDonald, L. Zuin, and J. Sanderson, J. Phys. B **49**, 215602 (2016).
[18] Z. Shen, E. Wang, M. Gong, X. Shan, and X. Chen, J. Chem. Phys. **145**, 234303 (2016).
[19] J. Laksman, D. Céolin, M. Gisselbrecht, and S. L. Sorensen, J. Chem. Phys. **133**, 144314 (2010).
[20] H. Ohmura, N. Saito, and T. Morishita, Phys. Rev. A **89**, 013405 (2014).
[21] B. Wales, É. Bisson, R. Karimi, S. Beaulieu, A. Ramadhan, M. Giguère, Z. Long, W.-K. Liu, J.-C. Kieffer, F. Légaré, and J. Sanderson, J. Electron Spectrosc. Relat. Phenom. **195**, 332 (2014).
[22] J. H. Sanderson, T. R. J. Goodworth, A. El-Zein, W. A. Bryan, W. R. Newell, A. J. Langley, and P. F. Taday, Phys. Rev. A **65**, 043403 (2002).

[23] W. A. Bryan, W. R. Newell, J. H. Sanderson, and A. J. Langley, Phys. Rev. A **74**, 053409 (2006).
[24] Y. Sakemi, S. Minemoto, and H. Sakai, Phys. Rev. A **96**, 011401(R) (2017).
[25] S. Luo, W. Hu, J. Yu, R. Zhu, L. He, X. Li, P. Ma, C. Wang, F. Liu, W. G. Roeterdink, S. Stolte, and D. Ding, J. Phys. Chem. A **121**, 777 (2017).
[26] L. He, J. Bulthuis, S. Luo, J. Wang, C. Lu, S. Stolte, D. Ding, and W. G. Roeterdink, Phys. Chem. Chem. Phys. **17**, 24121 (2015).
[27] J. Ullrich, R. Moshammer, A. Dorn, R. Dörner, L. Ph. H. Schmidt, and H. Schmidt-Böcking, Rep. Prog. Phys. **66**, 1463 (2003).
[28] X. Li, C. Wang, Z. Yuan, D. Ye, P. Ma, W. Hu, S. Luo, L. Fu, and D. Ding, Phys. Rev. A **96**, 033416 (2017).
[29] J. L. Chaloupka, J. Rudati, R. Lafon, P. Agostini, K. C. Kulander, and L. F. DiMauro, Phys. Rev. Lett. **90**, 033002 (2003).
[30] H. Ren, M. R. Provorse, P. Bao, Z. Qu, and J. Gao, J. Phys. Chem. Lett. **7**, 2286 (2016).
[31] A. Grofe, Z. Qu, D. G. Truhlar, H. Li, and J. Gao, J. Chem. Theory Comput. **13**, 1176 (2017).
[32] C. Bomme, R. Guillemin, T. Marin, L. Journel, T. Marchenko, N. Trcera, R. K. Kushawaha, M. N. Piancastelli, M. Simon, M. Stener, and P Decleva, J. Phys. B **45**, 194005 (2012).
[33] V. Brites, J. H. D. Eland, and M. Hochlaf, Chem. Phys. **346**, 23 (2008).
[34] I. A. Bocharova, A. S. Alnaser, U. Thumm, T. Niederhausen, D. Ray, C. L. Cocke, and I. V. Litvinyuk, Phys. Rev. A **83**, 013417 (2011).
[35] A. J. Cohen, P. Mori-Sánchez, and W. Yang, Science **321**, 792 (2008).
[36] S. Larimian, S. Erattupuzha, S. Mai, P. Marquetand, L. González, A. Baltuška, M. Kitzler, and X. Xie, Phys. Rev. A **95**, 011404(R) (2017).
[37] A. S. Alnaser, X. M. Tong, T. Osipov, S. Voss, C. M. Maharjan, P. Ranitovic, B. Ulrich, B. Shan, Z. Chang, C. D. Lin, and C. L. Cocke, Phys. Rev. Lett. **93**, 183202 (2004).
[38] C. Wu, Y. Yang, Z. Wu, B. Chen, H. Dong, X. Liu, Y. Deng, H. Liu, Y. Liu, and Q. Gong, Phys. Chem. Chem. Phys. **13**, 18398 (2011).